ISSN 0023-1584, Kinetics and Catalysis, 2012, Vol. 53, No. 5, pp. 620–631. © Pleiades Publishing, Ltd., 2012.
Original Russian Text © P.A. Nikul'shin, A.V. Mozhaev, D.I. Ishutenko, P.P. Minaev, A.I. Lyashenko, A.A. Pimerzin, 2012, published in Kinetika i Kataliz, 2012, Vol. 53, No. 5, pp. 660–672.

RUSSIAN CONGRESS ON CATALYSIS
"ROSKATALIZ"

Influence of the Composition and Morphology of Nanosized Transition Metal Sulfides Prepared Using the Anderson-Type Heteropoly Compounds $[X(OH)_6Mo_6O_{18}]^{n-}$ (X = Co, Ni, Mn, Zn) and $[Co_2Mo_{10}O_{38}H_4]^{6-}$ on Their Catalytic Properties

P. A. Nikul'shin, A. V. Mozhaev, D. I. Ishutenko, P. P. Minaev, A. I. Lyashenko, and A. A. Pimerzin

Samara State Technical University, Samara, 443010 Russia

e-mail: A.P.Nikulshin@gmail.com

Received October 28, 2011

Abstract—Using the Anderson-type heteropoly compounds (HPCs) $[X(OH)_6Mo_6O_{18}]^{n-}$ (X = Co, Ni, Mn, Zn) and $[Co_2Mo_{10}O_{38}H_4]^{6-}$ and cobalt (or nickel) nitrate, XMo/Al_2O_3 and $Co(Ni)–XMo/Al_2O_3$ catalysts were prepared. The catalysts were studied by low-temperature nitrogen adsorption, X-ray diffraction, and high-resolution transmission electron microscopy. The average length of the active-phase particles of the catalysts was 3.5 to 3.9 nm, and the average number of MoS_2 layers in a packet was 1.4 to 2.1. The catalytic properties of the samples, which were estimated in dibenzothiophene (DBT) hydrodesulfurization and in the hydrotreating of the diesel fraction, are considerably dependent upon both the type and composition of the HPC, and the nature of the applied promoter (Ni or Co). As compared to the Ni-promoted catalysts, the Co-promoted samples exhibit a higher desulfurization activity, whereas the hydrogenation ability of the $Ni–XMo/Al_2O_3$ catalysts surpasses that of the $Co–XMo/Al_2O_3$ ones. The catalytic properties depend on the morphology of the nanostructured active phase. With a growing number of MoS_2 layers in the packet of the catalysts' active phase, the DBT hydrodesulfurization rate constants for both the direct desulfurization route and the preliminary hydrogenation rote rise linearly and the selectivity falls linearly for the hydrogenation route. The selectivity of $Ni–XMo/Al_2O_3$ decreases to a greater extent than that of $Co–XMo/Al_2O_3$. The dependences of the catalytic properties on the morphology of the catalysts' active phase are consistent with the "dynamic" model of the functioning of the active sites of transition metal sulfides.

DOI: 10.1134/S0023158412050114

INTRODUCTION

Production of ultrapure diesel fuels by their deep hydrotreating in the presence of catalysts based on transition metal sulfides is becoming particularly important due to the introduction of new, more stringent environmental regulations in many countries all over the world [1].

Sulfide catalysts of the $Ni(Co)Mo(W)/Al_2O_3$ type are widely used in the hydrotreating of various petroleum stocks. Although this type of catalyst have been employed for over 70 years, the composition and structure of the catalysts' active phase and active sites, which influence the catalysis of hydrodesulfurization (HDS) and hydrogenation (HYD) reactions considerably, have been studied rather poorly and are still the subject of scientific investigation. To describe the active phase and the structure of active sites of hydrotreating catalysts, different models were proposed [2–5]. At present, it is generally recognized that the synergism of the catalytic action of Co(Ni) and Mo sulfides is due to the formation of a Co(Ni)MoS phase in which finely dispersed MoS_2 crystallites are decorated with promoter atoms (Co or Ni). At least two types of active components are distinguished in the sulfide catalysts, namely, Co(Ni)MoS phases of types I and II [1, 3, 6, 7]. The type II CoMoS phase is far superior to the type I phase in activity [2, 3, 6–9]. The type II Co(Ni)MoS phase features weak interaction between the active components and the support and, accordingly, a greater degree of sulfiding [6–9]. In most cases, type II phases are in the form of multilayered MoS_2 packets [1, 2, 10], although this feature may be missing [11].

In recent years, techniques of selective formation of the type II Co(Ni)MoS phase on the support surface have been employed to devise new hydrotreating catalysts [1, 4, 10]. The morphology of crystallites of the resulting active phase (orientation on the support, length, and number of MoS_2 layers in a packet) affects the catalysts' properties considerably [1, 5, 11, 12]. The development of ways of controlling the geometry of the active component is an important line of research in sulfide catalysis.

The most widespread synthetic technique to produce the type II Co(Ni)MoS phase is employing organic chelating agents like nitrilotriacetic or ethylenediaminetetraacetic acid [13–25], new or modified alumina supports weakly interacting with the precursor and then with the catalyst's active phase itself [26–32], and new initial compounds [33–56] for preparing catalysts. Use of different heteropoly compounds (HPCs) as active-phase precursors is of special interest [10, 35–56]. As we showed earlier, the nature of the heteroatom in a HPC with an Anderson structure considerably affects the catalytic properties of transition metal sulfides in thiophene hydrogenolysis, benzene hydrogenation, and hydrotreating of diesel fractions [53–55]. The catalysts synthesized using HPCs with the general formula $[X(OH)_6Mo_6O_{18}]^{n-}$ (or XMo_6HPC), where X = Co, Ni, Mn, or Zn, proved to be the most active [53]. When using Ni_x–XMo_6HPC/Al_2O_3 catalysts promoted with additional Ni, different synergistic effects were observed in benzene hydrogenation and thiophene hydrogenolysis [53]. It was established that, to obtain highly active catalysts for hydrotreating, it is preferable to use $[Co_2Mo_{10}O_{38}H_4]^{6-}$ ($Co_2Mo_{10}HPC$), whose structure is a derivative from the Anderson structure, rather than $Co(Ni)Mo_6HPC$ [46, 51, 52, 54].

The aim of the present work was to study the correlation between the composition, morphology, and catalytic properties of nanosized transition metal sulfides prepared using the Anderson-type HPCs $[X(OH)_6Mo_6O_{18}]^{n-}$ (X = Co, Ni, Mn, Zn) and $[Co_2Mo_{10}O_{38}H_4]^{6-}$ in dibenzothiophene HDS and in the hydrotreating of the diesel fraction.

EXPERIMENTAL

Synthesis of the Co(Ni)–XMo/Al_2O_3 Catalysts

Anderson-type ammonium salts of heteropoly acids with then general formula $(NH_4)_{6-x}[X_x(OH)_6Mo_6O_{18}] \cdot nH_2O$, where the central heteroatom X is Mn(II), Ni(II), Co(II), or Zn(II), and $Co_2Mo_{10}HPC$ were synthesized via standard or modified procedures [57–60].

As a support, γ-Al_2O_3 with a specific surface area of 230 m^2/g, a specific pore volume of 0.755 cm^3/g, and an effective pore radius of 124 Å was used. The $Co(Ni)$–XMo/Al_2O_3 catalysts were prepared by impregnation of the support (size fraction of 0.25 to 0.5 mm) with solutions of XMo_6HPC and $Ni(NO_3)_2 \cdot 6H_2O$ (reagent grade) (hereafter, the prepared samples are designated as Ni_x–XMo_6HPC/Al_2O_3), XMo_6HPC and $Co(NO_3)_2 \cdot 6H_2O$ (chemically pure) (hereafter, Co_x–XMo_6HPC/Al_2O_3), $Co_2Mo_{10}HPC$ and $Ni(NO_3)_2 \cdot 6H_2O$ (hereafter, Ni_3–$Co_2Mo_{10}HPC/Al_2O_3$), and $Co_2Mo_{10}HPC$ and $Co(NO_3)_2 \cdot 6H_2O$ (hereafter, Co_3-$Co_2Mo_{10}HPC/Al_2O_3$) with 10% hydrogen peroxide. XMo_6HPC/Al_2O_3 catalysts based on XMo_6HPC were obtained for comparison. The calculated Mo content of the catalysts was 10 wt %, and their Co (or Ni) content was 3 wt %.

The catalysts were dried at 80, 100, and 120°C for 2 h at each temperature. Then they were sulfided. For this purpose, the catalyst size fraction of 0.25 to 0.50 mm was impregnated with a sulfiding agent—di-*tert*-butyl polysulfide (sulfur content of 54 wt %), placed in a reactor, and treated with an H_2S–H_2 mixture (20 vol % H_2S) at atmospheric pressure and a temperature of 400°C for 2 h.

The metal content of the catalysts was determined with an EDX800HS X-ray fluorescence analyzer. The sulfur content was determined both before and after testing the catalyst in a flow reactor, and the coke content was determined in spent catalysts (Table 1) [61].

Determining the Physicochemical Properties of the Catalysts

The textural properties of the support and catalysts were determined using an Autosorb-1 adsorption porosimeter (Quantachrome) by low-temperature nitrogen adsorption. The specific surface area was calculated using the Brunauer–Emmett–Teller adsorption technique at a relative partial pressure P/P_0 from 0.05 to 0.3. The total pore volume and pore radius distribution were found by analyzing the desorption curve within the Barrett–Joyner–Halenda model.

X-ray diffraction patterns were were obtained on an ARLX'TRA diffractometer (Thermo Fisher Scientific) using CuK_α radiation ($\lambda = 1.54$ Å, 38 mA, 43 kV, scan speed of 2 deg/min).

High-resolution transmission electron microscopy (HRTEM) was carried out using a Technai G2 20F (FEI Company) instrument with a LaB_6 cathode at an accelerating voltage of 200 kV and a Technai G2 30F instrument with a LaB_6 cathode at an accelerating voltage of 300 kV. Catalyst samples were applied to a copper grid coated with a carbon film. TEM images were recorded in the bright field mode under underfocusing conditions with no objective aperture (phase contrast) at a magnification of 200000. The average MoS_2 crystallite size and the number of MoS_2 layers in an active-phase packet were estimated by calculations performed for over 500 particles situated on 10 to 15 different surface patches.

Catalytic Properties of the Catalysts

The catalytic properties of the synthesized catalysts in the DBT hydrodesulfurization reaction were studied on a microflow unit. A catalyst (0.3 g, size fraction of 0.25 to 0.5 mm) diluted with 1 cm^3 of silicon carbide SiC with a particle size of 0.2 to 0.4 mm was charged into a tubular reactor with an inner diameter of 8 mm. A solution of DBT in *n*-heptane (sulfur content of 0.15 wt %) was used as the feedstock. The experiments were conducted under the following conditions: feed hourly space velocity of 10.0 h^{-1}, reaction temperature of 250°C, pressure of 3.0 MPa, and hydrogen-to-feedstock ratio of 700 nL/L. The liquid catalyzate was

sampled from a low-pressure separator and was analyzed on a Kristall-5000 gas chromatograph (capillary column OV-101) every half-hour. The reaction products were identified as the retention times of commercially available standards and by the GC-MS method using a Finnigan Trace DSQ instrument. In order to evaluate the degree of inactivation of catalysts, every experiment lasted for 10 h. All of the samples retained their activity and selectivity after 5- to 6-h-long continuous testing.

The first-order DBT HDS reaction rate constant (k_{HDS}) was found from the equation

$$k_{HDS} = -\frac{F}{W}\ln(1-x),$$

where k_{HDS} is the first-order reaction rate constant (mol g^{-1} h^{-1}), x is the DBT conversion (%), F is the DBT flow rate (mol/h), and W is the catalyst mass (g). The main products of DBT HDS were biphenyl (BP) resulting direct DBT desulfurization (DS) and cyclohexylbenzene (CHB) and dicyclohexyl (DCH) formed via DBT hydrogenation (HYD). Trace amounts of the products of incomplete DBT (or tetrahydrodibenzothiophene, THDBT) hydrogenation were found on all catalysts. The selectivity $S_{HYD/DS}$ was calculated according to the scheme

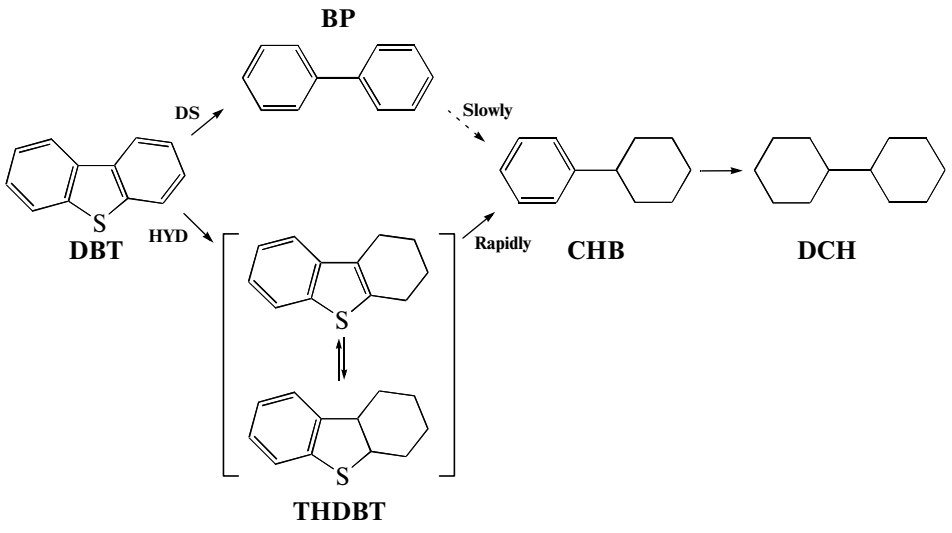

using the following equation:

$$S_{HYD/DS} = \frac{k_{HYD}}{k_{DS}} = \frac{C_{CHB} + C_{DCH}}{C_{BP}},$$

where C_{CHB}, C_{DCH}, and C_{BP} are the cyclohexylbenzene, dicyclohexyl, and biphenyl contents of the reaction products (in weight percent).

The catalysts were also tested in the hydrotreating of a mixture of 20 vol % light cat-cracked gas-oil and 80 vol % straight-run diesel fraction obtained at OAO Syzran Refinery. The laboratory flow unit included temperature, pressure, and hydrogen-containing gas and feedstock flow rate control blocks. The temperature, pressure, and feedstock and hydrogen flow rates were maintained with an accuracy of ±1°C, ±0.05 MPa, ±0.1 cm^3/h, and ±0.2 L/h, respectively. The testing was performed at temperatures of 320, 340, and 360°C, a pressure of 4.0 MPa, a feedstock hourly space velocity of 2.0 h^{-1}, a hydrogen-to-feedstock ratio of 500 nL/L, and a catalyst volume of 10 cm^3.

The resulting hydrogenation products were sampled once in 1–2 h until a constant sulfur content was obtained under the preset process conditions. The samples were treated with a 15% NaOH solution for 15 min to remove dissolved hydrogen sulfide. The treated samples were washed with distilled water until neutral and were dried with calcium chloride.

The sulfur content of the hydrogenation products was evaluated on an EDX800HS X-ray fluorescence energy-dispersive spectrometer (Shimadzu). For quantitative determination of polycyclic aromatic hydrocarbons (PAHs) content, a UV-1700 spectrophotometer (Shimadzu) was used [61].

The activity of the catalysts in the hydrodesulfurization process (HDS activity) was estimated using the formula

$$x_S = \frac{[S]_f - [S]_h}{[S]_f} \times 100\%,$$

where x_S is the degree of hydrodesulfurization (%), $[S]_f$ is the sulfur content of the feedstock (wt %), and $[S]_h$ is the sulfur content of the hydrogenation product (wt %). The catalytic activity in polycyclic aromatic hydrocarbon hydrogenation (HYD activity) was estimated using the expression

$$x_{PAH} = \frac{[Ar]_f - [Ar]_h}{[Ar]_f} \times 100\%,$$

where x_{PAH} is the degree of PAH hydrogenation (%), $[Ar]_f$ is the PAH content of the feedstock (wt %), and

Table 1. Composition of the Co(Ni)–XMo/Al_2O_3 catalysts

Precursors of active components	Catalyst designation	Content, wt %				$\frac{Co(Ni)}{Co(Ni)+Mo}$	Coke content*, wt %
		Mo	Ni	Co	S		
$(NH_4)_4[Ni(OH)_6Mo_6O_{18}]$	$NiMo_6HPC/Al_2O_3$	10.0	0.9	–	6.8	0.13	–
$(NH_4)_4[Mn(OH)_6Mo_6O_{18}]$	$MnMo_6HPC/Al_2O_3$	9.9	–	–	6.7	–	–
$(NH_4)_4[Zn(OH)_6Mo_6O_{18}]$	$ZnMo_6HPC/Al_2O_3$	9.9	–	–	6.6	–	–
$(NH_4)_4[Co(OH)_6Mo_6O_{18}]$	$CoMo_6HPC/Al_2O_3$	10.1	–	1.0	7.0	0.14	–
$(NH_4)_6[Co_2Mo_{10}O_{38}H_4]$	$Co_2Mo_{10}HPC/Al_2O_3$	10.0	–	1.2	7.2	0.17	–
$Ni(NO_3)_2 + (NH_4)_4[Ni(OH)_6Mo_6O_{18}]$	$Ni_2–NiMo_6HPC/Al_2O_3$	10.0	3.2	–	7.7	0.33	1.2
$Ni(NO_3)_2 + (NH_4)_4[Mn(OH)_6Mo_6O_{18}]$	$Ni_3–MnMo_6HPC/Al_2O_3$	9.9	2.9	–	7.9	0.32	3.6
$Ni(NO_3)_2 + (NH_4)_4[Zn(OH)_6Mo_6O_{18}]$	$Ni_3–ZnMo_6HPC/Al_2O_3$	9.8	3.0	–	7.8	0.33	2.0
$Ni(NO_3)_2 + (NH_4)_4[Co(OH)_6Mo_6O_{18}]$	$Ni_2–CoMo_6HPC/Al_2O_3$	9.9	2.1	1.0	7.9	0.34	1.1
$Ni(NO_3)_2 + (NH_4)_6[Co_2Mo_{10}O_{38}H_4]$	$Ni_3–Co_2Mo_{10}HPC/Al_2O_3$	10.0	1.8	1.2	8.0	0.32	1.3
$Co(NO_3)_2 + (NH_4)_4[Ni(OH)_6Mo_6O_{18}]$	$Co_2–NiMo_6HPC/Al_2O_3$	10.0	1.0	2.0	7.8	0.33	2.0
$Co(NO_3)_2 + (NH_4)_4[Mn(OH)_6Mo_6O_{18}]$	$Co_3–MnMo_6HPC/Al_2O_3$	9.9	–	3.0	7.7	0.33	4.2
$Co(NO_3)_2 + (NH_4)_4[Zn(OH)_6Mo_6O_{18}]$	$Co_3–ZnMo_6HPC/Al_2O_3$	10.1	–	3.1	7.7	0.33	2.4
$Co(NO_3)_2 + (NH_4)_4[Co(OH)_6Mo_6O_{18}]$	$Co_2–CoMo_6HPC/Al_2O_3$	10.0	–	3.0	7.8	0.33	1.3
$Co(NO_3)_2 + (NH_4)_6[Co_2Mo_{10}O_{38}H_4]$	$Co_3–Co_2Mo_{10}HPC/Al_2O_3$	10.0	–	2.9	7.9	0.32	1.0

* After testing the catalyst in the hydrotreating of the diesel fractions.

$[Ar]_h$ is the PAH content of the hydrogenation product (wt %).

RESULTS AND DISCUSSION

Physicochemical Properties of the Catalysts

The composition of the synthesized catalysts is given in Table 1. The Co(Ni) : Mo molar ratio was ~0.33 in the promoted catalysts Co(Ni)–XMo/Al_2O_3. This is the value at which the maximal synergistic effect is observed, according to most authors [1–4]. The sulfur content of the sulfided samples was 7.7 to 8.0 wt %, indicating a high degree of metal sulfiding.

After the oxide precursors were supported and the catalysts were sulfided, the specific surface area and specific pore volume decreased by 17 to 33% as compared to the same characteristics of the initial γ-Al_2O_3 support (Table 2). As this took place, the average pore radius decreased by 0.5 to 1.5 Å. The character of the pore size distribution in the sulfide catalysts remained the same as in the initial support, which was evidence of uniform surface coverage with the active-phase components (Fig. 1).

The diffraction patterns of the synthesized catalysts in the sulfided state are shown in Fig. 2. The samples consist of only the low-temperature γ-Al_2O_3 phase (PDF No. 48-367). The absence of reflections from bulk transition metal sulfides or any oxysulfide species suggests that the active phase is amorphous or ultradispersed.

The TEM images of several sulfide catalysts are presented in Fig. 3. The average length of the active-phase particles and the average number of MoS_2 layers per packet for the synthesized samples are given in Table 3. The dark threadlike lines in the TEM images represent layers of MoS_2 crystallites. The interplanar spacing in these crystallites is about 0.62 nm, characteristic of the basal plane (002) of crystalline MoS_2 [2, 4, 11]. The images of the surface of the synthesized catalysts do not show any Co_xS_y or Ni_xS_y crystallites. The average length $\overline{L}$ of the active-component particles varies between 3.5 and 3.9 nm, and the average number of MoS_2 layers in a packet is $\overline{N} = 1.4–2.1$. The greatest $\overline{N}$ values were observed for the catalysts $Co_3–Co_2Mo_{10}HPC/Al_2O_3$ and $Ni_3–Co_2Mo_{10}HPC/Al_2O_3$; the smallest value, for $ZnMo_6HPC/Al_2O_3$. These morphological features of the catalysts' active phase are typical of the type II Co(Ni)MoS multilayered phase [11, 12, 22, 24, 26, 27]. In the Co(Ni)–XMo/Al_2O_3

Table 2. Textural properties of the support and synthesized catalysts

Object	Specific surface area, m^2/g	Specific pore volume, cm^3/g	Average pore radius, Å
Al_2O_3	230	0.755	62.0
$NiMo_6HPC/Al_2O_3$	190	0.592	61.3
$MnMo_6HPC/Al_2O_3$	187	0.587	61.4
$ZnMo_6HPC/Al_2O_3$	188	0.591	61.4
$CoMo_6HPC/Al_2O_3$	190	0.590	61.5
$Co_2Mo_{10}HPC/Al_2O_3$	184	0.585	61.5
$Ni_2–NiMo_6HPC/Al_2O_3$	167	0.554	61.0
$Ni_3–MnMo_6HPC/Al_2O_3$	175	0.548	61.0
$Ni_3–ZnMo_6HPC/Al_2O_3$	173	0.550	61.5
$Ni_2–CoMo_6HPC/Al_2O_3$	167	0.555	61.0
$Ni_3–Co_2Mo_{10}HPC/Al_2O_3$	170	0.558	61.0
$Co_2–NiMo_6HPC/Al_2O_3$	174	0.556	60.5
$Co_3–MnMo_6HPC/Al_2O_3$	172	0.554	61.0
$Co_3–ZnMo_6HPC/Al_2O_3$	175	0.545	61.0
$Co_2–CoMo_6HPC/Al_2O_3$	165	0.551	61.5
$Co_3–Co_2Mo_{10}HPC/Al_2O_3$	170	0.538	61.5

Table 3. Characteristics of the active phase of the XMo/Al_2O_3 and $Co(Ni)–XMo/Al_2O_3$ catalysts

Catalyst	Number of MoS_2 packets per 1000 nm^2	$\overline{L}$, nm	$\overline{N}$
$NiMo_6HPC/Al_2O_3$	35	3.6	1.6
$MnMo_6HPC/Al_2O_3$	36	3.5	1.5
$ZnMo_6HPC/Al_2O_3$	34	3.6	1.4
$CoMo_6HPC/Al_2O_3$	33	3.7	1.7
$Co_2Mo_{10}HPC/Al_2O_3$	34	3.5	1.8
$Ni_2–NiMo_6HPC/Al_2O_3$	32	3.8	1.8
$Ni_3–MnMo_6HPC/Al_2O_3$	31	3.5	1.7
$Ni_3–ZnMo_6HPC/Al_2O_3$	34	3.8	1.6
$Ni_2–CoMo_6HPC/Al_2O_3$	31	3.8	1.9
$Ni_3–Co_2Mo_{10}HPC/Al_2O_3$	36	3.7	2.1
$Co_2–NiMo_6HPC/Al_2O_3$	32	3.9	1.7
$Co_3–MnMo_6HPC/Al_2O_3$	29	3.7	1.7
$Co_3–ZnMo_6HPC/Al_2O_3$	30	3.9	1.6
$Co_2–CoMo_6HPC/Al_2O_3$	29	3.8	1.8
$Co_3–Co_2Mo_{10}HPC/Al_2O_3$	34	3.8	2.0

catalysts promoted with cobalt and nickel, the values of $\overline{L}$ and $\overline{N}$ are greater than those in XMo/Al_2O_3.

Catalytic Properties of the Synthesized Samples

The results of investigation of the catalytic activity of the synthesized samples in the DBT HDS reaction are presented in Table 4. The DBT conversion was from about 7 to 34%. The conversion level was the lowest for the unpromoted XMo/Al_2O_3 catalysts. The rate constant k_{HDS} for these samples was from 7.2×10^{-5} to 15.6×10^{-5} mol g^{-1} h^{-1} (the maximal value was observed for $Co_2Mo_{10}HPC/Al_2O_3$; the minimal value, for $ZnMo_6HPC/Al_2O_3$). The XMo/Al_2O_3 catalysts exhibited a higher catalytic activity than the $Co(Ni)–XMo/Al_2O_3$ ones.

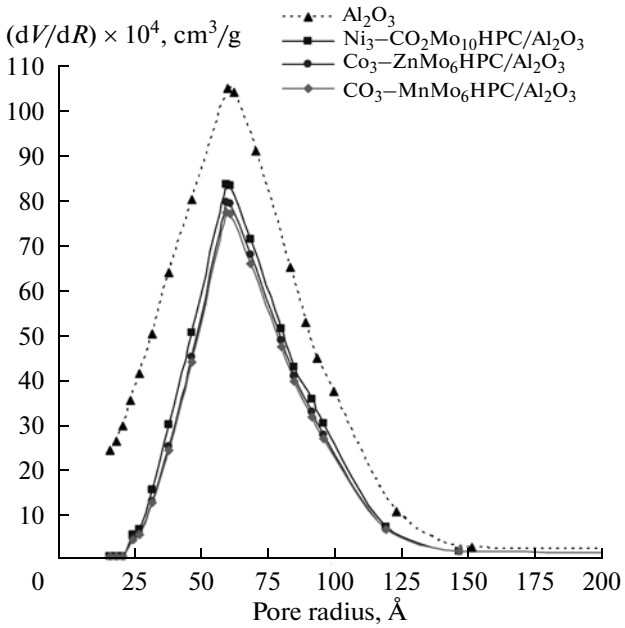

Fig. 1. Pore radius distribution in the support and in the Co_3–$MnMo_6HPC/Al_2O_3$, Co_3–$ZnMo_6HPC/Al_2O_3$, and Ni_3–$Co_2Mo_{10}HPC/Al_2O_3$ sulfide catalysts.

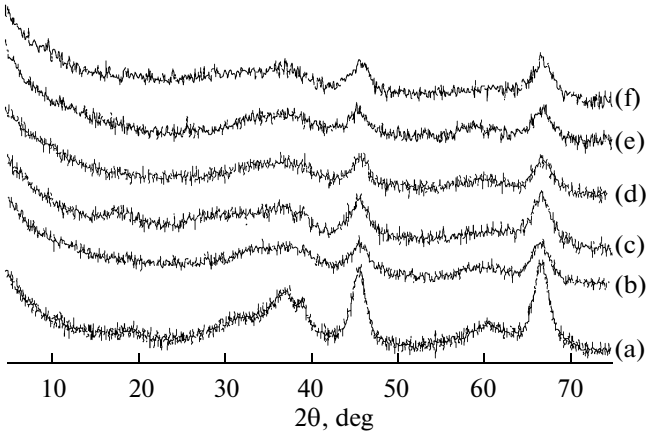

Fig. 2. Diffraction patterns of the support and sulfide catalysts: (a) γ-Al_2O_3 support, (b) Ni_2–$NiMo_6HPC/Al_2O_3$, (c) Ni_3–$MnMo_6HPC/Al_2O_3$, (d) Co_3–$MnMo_6HPC/Al_2O_3$, (e) Co_3–$ZnMo_6HPC/Al_2O_3$, and (f) Co_3–$Co_2Mo_{10}HPC/Al_2O_3$.

The rate constant k_{HDS} for the promoted catalysts Co(Ni)–XMo/Al_2O_3 was two or three times higher that that for XMo/Al_2O_3 (Fig. 4). The maximal synergistic effect was observed with Co_2–$NiMo_6HPC/Al_2O_3$, Ni_3–$MnMo_6HPC/Al_2O_3$, and Ni_3–$ZnMo_6HPC/Al_2O_3$. The Co-promoted catalysts showed a higher catalytic activity than the NiMo samples (Table 4). However, the rate constant k_{HYD} for the preliminary hydrogenation route (see the scheme) for the Ni–XMo/Al_2O_3 catalysts was larger than that for the Co–XMo/Al_2O_3. Therefore, the selectivity $S_{HYD/DS}$ of the Ni-promoted catalysts was 1.5–2 times higher than the selectivity of the Co-promoted samples.

The results of testing the catalysts in the hydrotreating of the diesel fractions are given in Table 5 and in Figs. 5 and 6. Under the catalyst testing conditions, the residual sulfur content of the stable hydrogenation products was 30 to 250 ppm, and their PAH content was 1.7 to 3.5 wt % (Table 5). With an increas-

Table 4. Catalytic properties of the synthesized samples in dibenzothiophene hydrodesulfurization

Catalyst	DBT conversion, %	Constant ×10^5, mol g^−1 h^−1			Selectivity $S_{HYD/DS}$
		k_{HDS}	k_{DS}	k_{HYD}	
$NiMo_6HPC/Al_2O_3$	8.0	8.9	6.1	2.8	0.46
$MnMo_6HPC/Al_2O_3$	7.5	8.3	5.5	2.8	0.52
$ZnMo_6HPC/Al_2O_3$	6.5	7.2	4.7	2.5	0.54
$CoMo_6HPC/Al_2O_3$	10.7	12.0	8.3	3.7	0.41
$Co_2Mo_{10}HPC/Al_2O_3$	13.6	15.6	10.9	4.7	0.43
Ni_2–$NiMo_6HPC/Al_2O_3$	16.4	19.1	13.6	5.5	0.43
Ni_3–$MnMo_6HPC/Al_2O_3$	17.2	20.1	14.2	6.0	0.45
Ni_3–$ZnMo_6HPC/Al_2O_3$	15.1	17.5	12.1	5.3	0.48
Ni_2–$CoMo_6HPC/Al_2O_3$	19.5	23.1	17.0	6.1	0.39
Ni_3–$Co_2Mo_{10}HPC/Al_2O_3$	27.2	33.9	25.1	8.8	0.38
Co_2–$NiMo_6HPC/Al_2O_3$	23.0	27.9	22.4	5.5	0.24
Co_3–$MnMo_6HPC/Al_2O_3$	19.5	23.1	18.3	4.8	0.26
Co_3–$ZnMo_6HPC/Al_2O_3$	17.7	20.8	16.3	4.5	0.27
Co_2–$CoMo_6HPC/Al_2O_3$	26.0	32.1	26.5	5.7	0.21
Co_3–$Co_2Mo_{10}HPC/Al_2O_3$	34.4	45.0	36.1	8.8	0.24

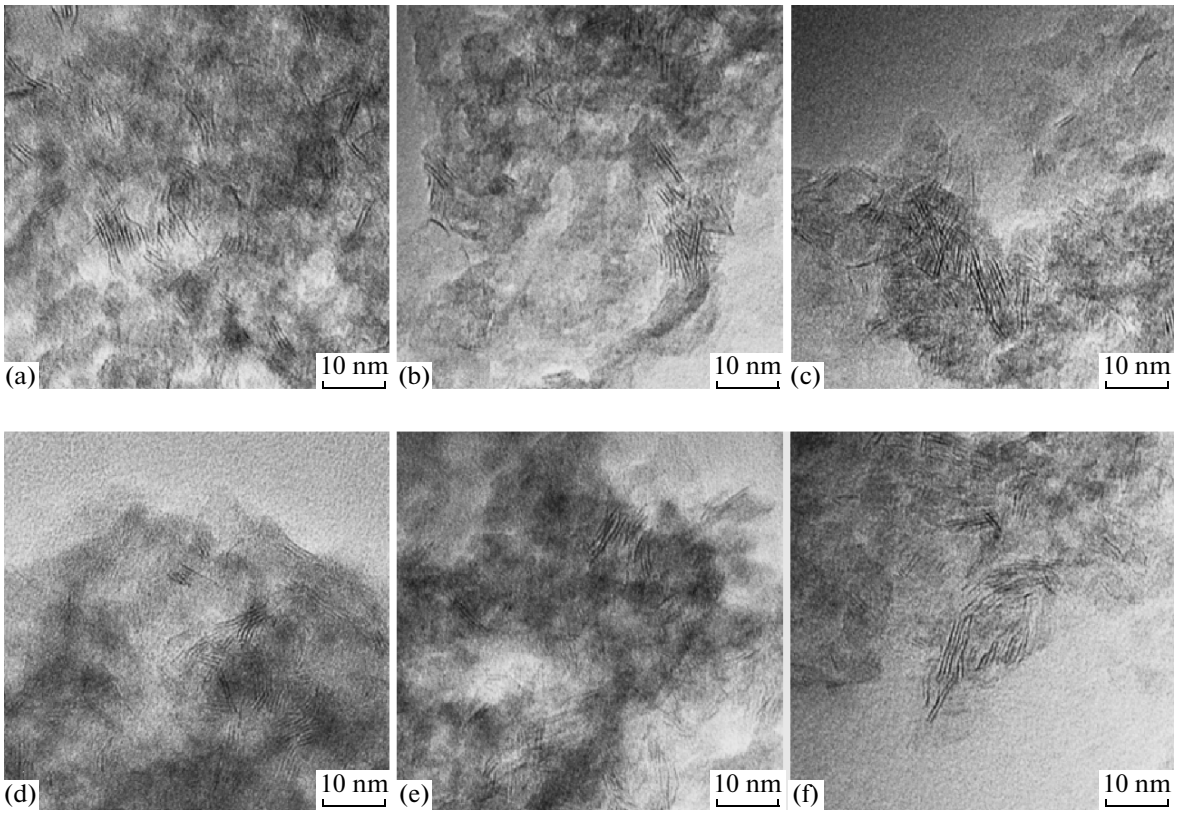

Fig. 3. TEM images of the Ni-promoted catalysts (a) Ni_2–$NiMo_6HPC/Al_2O_3$, (b) Ni_3–$ZnMo_6HPC/Al_2O_3$, and (c) Ni_3–$Co_2Mo_{10}HPC/Al_2O_3$ and Co-promoted catalysts (d) Co_2–$NiMo_6HPC/Al_2O_3$, (e) Co_3–$ZnMo_6HPC/Al_2O_3$, and (f) Co_3–$Co_2Mo_{10}HPC/Al_2O_3$.

ing temperature, the sulfur content of the stable hydrogenation products decreases because the HDS reactions are kinetically controlled, while their PAH content increases due to thermodynamic limitations [2, 61].

The Co-promoted catalysts Co_x–XMo_6HPC/Al_2O_3 exhibited greater HDS activity in the hydrotreating of the diesel oil fractions than Ni_x–XMo_6HPC/Al_2O_3 (Fig. 5a). The difference is 0.3 to 0.8%, which is equivalent to a 30–70 ppm change in the residual sulfur content of the stable hydrogenation products (Table 5), depending on the compound used in synthesis of the HPC catalyst with the Anderson structure. The maximal difference between the HDS activities of Co- and Ni-promoted catalysts was observed with $CoMo_6HPC$; the minimal difference, with $NiMo_6HPC$. Of the $Co(Ni)_x$–XMo_6HPC/Al_2O_3 samples, Co_2–$CoMo_6HPC/Al_2O_3$ showed the greatest HDS activity and Ni_2–$NiMo_6HPC/Al_2O_3$ and Ni_2–$CoMo_6HPC/Al_2O_3$ had the lowest HDS activity.

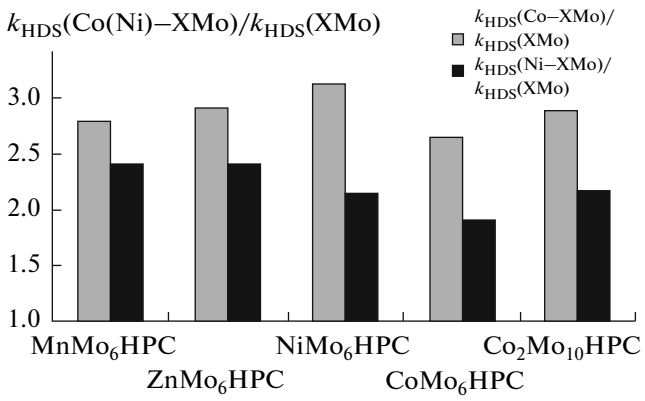

Fig. 4. Synergistic effect of the promotion of the XMo/Al_2O_3 catalysts with Co and Ni in dibenzothiophene hydrodesulfurization.

In the hydrotreating of the diesel fraction, the HYD activity of Ni_x–XMo_6HPC/Al_2O_3 was above that of Co_x–XMo_6HPC/Al_2O_3 for PAH hydrogenation (Fig. 5b). The difference was 1.3 to 3.0%, depending on the compound used in synthesis of the HPC catalyst. Of the catalysts promoted with Ni and Co, those synthesized with $CoMo_6HPC$ differed in both HDS and HYD activity most greatly and those prepared using $ZnMo_6HPC$ differed from one another to the smallest extent. Of the Ni_2–$NiMo_6$samples, the HYD activity of Al_2O_3 was the greatest and that of $Co(Ni)_x$–XMo_6 was the lowest.

In the $Ni(Co)$–XMo/Al_2O_3 catalyst series, the Co_3–$MnMo_6$ sample exhibited the greatest HDS

Table 5. Properties of the hydrogenation products obtained by hydrotreating the mixed diesel fraction over the Co(Ni)–XMo/Al_2O_3 catalysts

Catalyst	Process temperature, °C	Content, wt %			
		sulfur	BAH[a]	TAH[b]	PAH[c]
Ni_2–$NiMo_6HPC/Al_2O_3$	320	0.0247	1.32	0.40	1.72
	340	0.0176	1.35	0.43	1.79
	360	0.0097	1.40	0.46	1.86
Ni_3–$MnMo_6HPC/Al_2O_3$	320	0.0228	1.53	0.40	1.93
	340	0.0147	1.81	0.46	2.27
	360	0.0090	2.01	0.55	2.55
Ni_3–$ZnMo_6HPC/Al_2O_3$	320	0.0217	1.66	0.40	2.06
	340	0.0144	1.70	0.53	2.23
	360	0.0085	1.98	0.58	2.56
Ni_2–$CoMo_6HPC/Al_2O_3$	320	0.0243	1.35	0.41	1.76
	340	0.0159	1.46	0.43	1.89
	360	0.0097	1.60	0.51	2.11
Ni_3–$Co_2Mo_{10}HPC/Al_2O_3$	320	0.0229	1.38	0.42	1.80
	340	0.0145	1.49	0.44	1.93
	360	0.0091	1.64	0.50	2.14
Co_2–$NiMo_6HPC/Al_2O_3$	320	0.0219	1.39	0.42	1.81
	340	0.0141	1.50	0.45	1.95
	360	0.0065	1.79	0.54	2.32
Co_3–$MnMo_6HPC/Al_2O_3$	320	0.0154	1.65	0.40	2.05
	340	0.0080	1.84	0.59	2.43
	360	0.0046	2.48	0.64	3.12
Co_3–$ZnMo_6HPC/Al_2O_3$	320	0.0129	1.75	0.45	2.21
	340	0.0070	1.77	0.57	2.34
	360	0.0036	2.82	0.65	3.48
Co_2–$CoMo_6HPC/Al_2O_3$	320	0.0163	1.43	0.44	1.87
	340	0.0088	1.62	0.55	2.16
	360	0.0047	1.94	0.56	2.50
Co_3–$Co_2Mo_{10}HPC/Al_2O_3$	320	0.0119	1.40	0.42	1.82
	340	0.0064	1.58	0.48	2.06
	360	0.0032	1.70	0.53	2.23

Note: BAH, TAH, and PAH are dicyclic, tricyclic, and polycyclic aromatic hydrocarbons, respectively. The sulfur, BAH, TAH, and PAH content of the feedstock was 1.1341, 7.71, 1.33, and 9.04 wt %, respectively.

activity (Fig. 6a) and the$_2O_3$ sample exhibited the greatest HYD activity (Fig. 6b).

Therefore, an increase in the cobalt content of the synthesized Ni(Co)–XMo/Al_2O_3 catalysts (Table 1) enhances their HDS activity and an increase in their nickel content enhances their HYD activity. After testing, less coke was deposited on the Ni-promoted catalysts than on the Co-promoted ones (Table 1), which is seemingly due to the higher ability of the former to hydrogenate the coke precursors.

When the catalyst compositions and metal contents are the same, the type of the heteropoly anion (HPA used) has a crucial effect on the catalytic properties. The Co_3–$Co_2Mo_{10}HPC/Al_2O_3$ catalyst exhibits higher HDS and HYD activities than Ni_2–$NiMo_6$. The catalyst prepared using the dimeric Anderson structure$_2O_3$ was earlier shown to be more active in the thiophene HDS reaction than the catalyst based on Ni(Co)Mo/Al_2O_3 [46, 52]. The enhancement of the synergistic effect of Co and Ni when Co is located

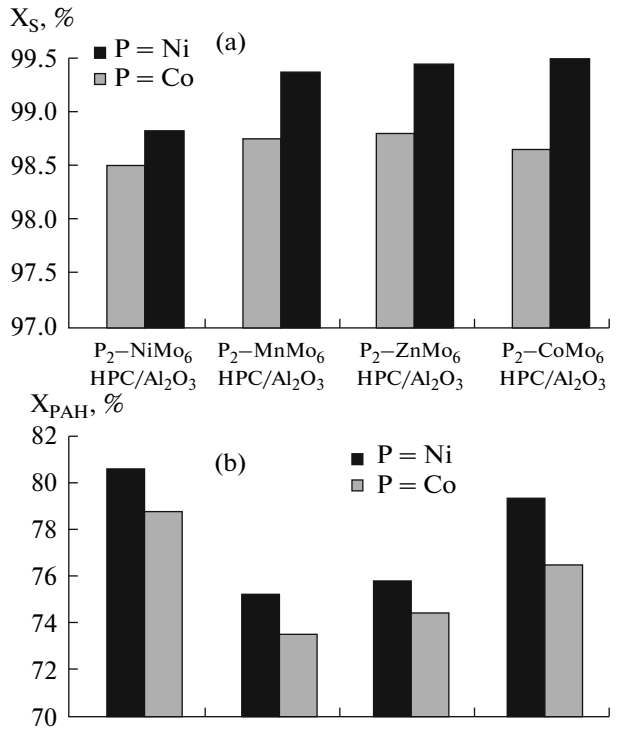

Fig. 5. (a) HDS activity and (b) HYD activity of $Co(Ni)_x$–XMo_6HPC/Al_2O_3 (X = Ni, Mn, Zn, Co) in the hydrotreating of the diesel fraction at 340°C.

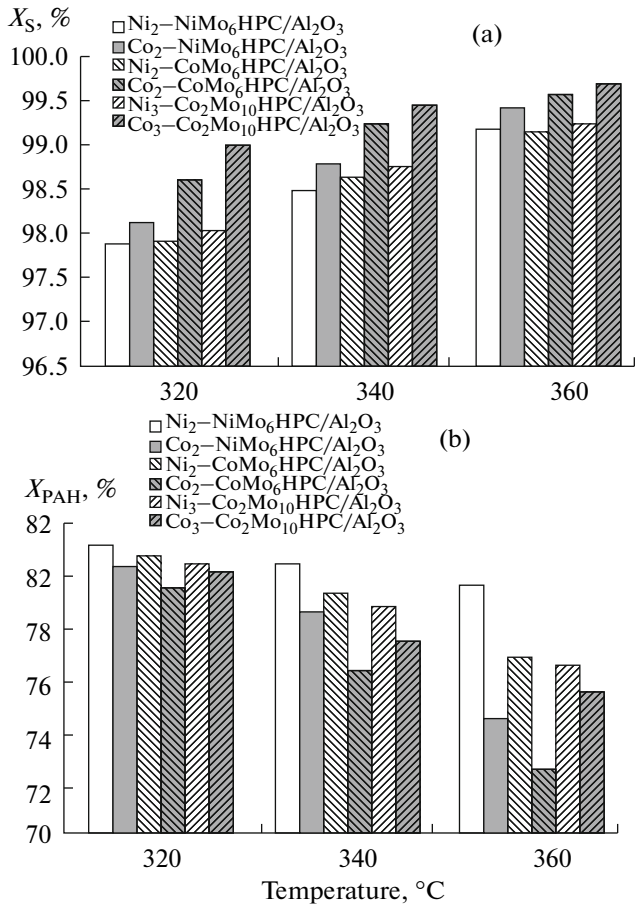

Fig. 6. (a) HDS activity and (b) HYD activity of $Co(Ni)_2$–$Ni(Co)Mo_6HPC/Al_2O_3$ and $Co(Ni)_3$–$Co_2Mo_{10}HPC/Al_2O_3$ in the hydrotreating of the diesel fraction at 320, 340, and 360°C.

within the HPA molecule can be owing to a close arrangement of the atoms inside the HPA. The spatial proximity of the promoter and Mo atoms was reported to be necessary for achieving high activity of sulfide catalysts for hydrotreating [62]. However, the HPA type has an effect on the morphology of the sulfide active phase (as shown in Table 3, the average number of MoS_2 layers in the Co_3–$Co_2Mo_{10}HPC/Al_2O_3$ packet is above that in Co_2–$CoMo_6HPC/Al_2O_3$) and, accordingly, on its catalytic properties.

Influence of the Morphology of the Active Phase on the Catalytic Properties of the Catalysts

During the sulfiding of the catalysts prepared using different HPCs, the decomposition of the HPA molecule takes place and the Mo (W) atoms turn into molybdenum or tungsten disulfide [38, 40, 42, 49, 51, 56, 61]. In this process, in the case of employing HPCs with a Keggin structure ($[PMo_{12}O_{40}]^{3-}$ or $[SiMo_{12}O_{40}]^{4-}$), the heteroatoms can migrate to the support surface in the form of individual oxides, for instance, P_2O_5 or SiO_2 [38, 42]. In the case of HPCs with the Anderson structure ($ZnMo_6HPC$, $MnMo_6HPC$, or $CoMo_6HPC$), they can get sulfided to yield separate particles of transition metal sulfides or oxysulfides [49, 53] or forming Co(Ni)–Mo–S active sites in case of the heteroatom being a promoter atom in $NiMo_6HPC$, $CoMo_6HPC$, or $Co_2Mo_{10}HPC$, capable of incorporating into the plane of S- or Mo-edge of MoS_2 and to get fixed on MoS_2 (WS_2) edges [49, 51, 61] due to its favorable geometry.

Under the XMo_6HPC/Al_2O_3 sulfiding conditions, MoS_2 particles performing the main catalytic function result. As this takes place, in the case of X = Zn and Mn, the heteroatom can form an individual finely dispersed sulfide (or oxysulfide) or, in the case of X = Co and Ni, it can incorporate into the MoS_2 edges, forming Co(Ni)–Mo–S sites, which are more active than the coordination-unsaturated sites (CUS's) in molybdenum disulfide. This provides an explanation for the order in which the activity of the catalysts unpromoted with extra Co (Ni) changes depending on the nature of the heteroatom: Zn < Mn < Ni < Co < Co_2 (Table 4). However, the nature of the heteroatom also affects the morphology of the MoS_2 particles and, accordingly, the concentration of active sites, i.e., Mo CUS's. In the catalyst based on $Co_2Mo_{10}HPC$, the maximal number of MoS_2 layers per packet was observed. Therefore, the second reason for the change in cata-

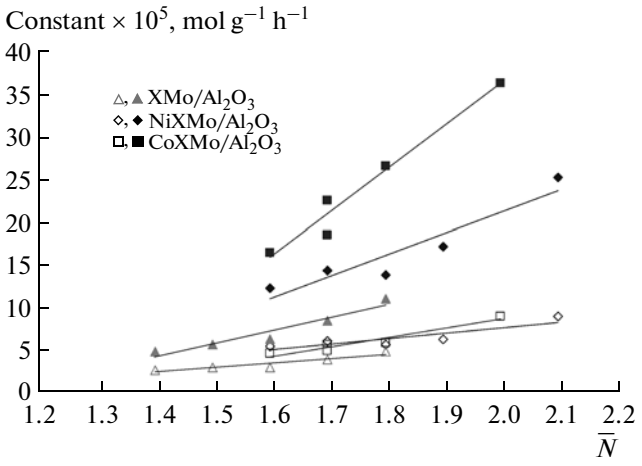

Fig. 7. Dependence of the dibenzothiophene hydrodesulfurization reaction rate constants on the average number of MoS_2 layers per packet for the direct desulfurization reaction route (closed circles) and hydrogenation reaction route (open circles).

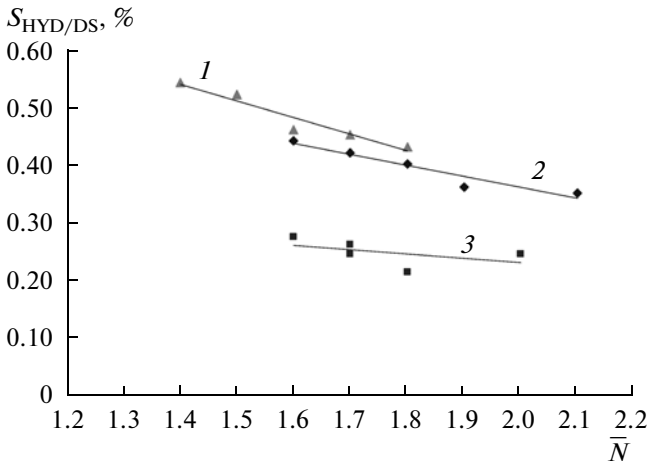

Fig. 8. Dependence of the selectivity of dibenzothiophene hydrodesulfurization on the average number of MoS_2 layers per packet for the hydrogenation reaction route over the catalysts (*1*) XMo/Al_2O_3, (*2*) $Ni–XMo/Al_2O_3$, and (*3*) $Co–XMo/Al_2O_3$.

lytic properties is the differences in the active-component morphology.

It is well-known that the maximal concentration of Co(Ni)–Mo–S sites and, accordingly, the highest specific catalytic activity is attained at a molar ratio of Mo : Co (Ni) ≈ 2 [1–5]. That is why, in order to diminish the influence of the initial HPC composition (nature of the heteroatom), we synthesized catalysts promoted with extra Ni (Co) with the same Mo and Co (Ni) contents, independent of the heteroatom type, and Mo : Co (Ni) ≈ 2.

The results obtained for these catalysts were used to relate the morphology of the active component to the catalytic properties of the samples. It was found that, as the number of MoS_2 layers per packet of the catalysts' active component increases from 1.4 to 2.1, the DBT HDS rate constant increases linearly (Fig. 7). At the same time, the selectivity $S_{HYD/DS}$ falls linearly as $\overline{N}$ increases (Fig. 8).

According to the "rim–edge" model [63–66], HDS and HYD sites identical in structure, but situated on "rims" and "edges" of MoS_2 crystallites, respectively, are recognized in the catalysts containing MoS_2 layers. The sites that are located on spatial angles (places of intersection of an edge and a "rim") of crystallites and are, therefore, the most coordination-unsaturated ones are the HYD sites. By changing the diameter-to-length ratio of the crystallite, one can vary the relative HDS and HYD site content and, therefore, the catalyst selectivity in the hydration and hydrodesulfurization reactions.

An increase in the rtate constant of direct DBT desulfurization (k_{DS}) with the number of MoS_2 layers per packet $\overline{N}$ (Fig. 7) is evidence that the HDS sites are actually situated on the active-phase crystallite edges, in conformance with the rim–edge model. According to this model, a rise in the crystallite rim length should lead to an increase in k_{HYD}. However, our results indicate no correlation between the active-phase particle length and k_{HYD} (Tables 3, 4). In addition, with growing $\overline{N}$, the DBT hydrogenation rate constant k_{HYD} for the catalysts XMo/Al_2O_3 and $Co(Ni)\text{-}XMo/Al_2O_3$ increases (Fig. 7), in contradiction to the rim–edge model. This confirms the recently proposed "dynamic" model of the performance of the active sites [5].

According to the dynamic model, the mechanism of catalysis by transition metal sulfides includes exchange stages involving sulfur atoms, promoter, hydrogen, and vacancies between CoMoS crystallite layers. The rate (frequency) of such movements characterizes the catalytic activity. The model implies that the change in the Co(Ni)MoS phase composition under the reaction conditions is due to the mobility of the sulfur and promoter atoms, which travel between molybdenum sulfide layers. According to the model considered, the HYD sites (or "slow" sites) are single clusters of unpromoted molybdenum sulfide, and desulfurization sites ("rapid" sites) are aggregates of two single molybdenum sulfide clusters of which one is promoted by Ni or Co. In this model, the HDS and HYD sites are considered to be located both on the rims and edges of the active-phase crystallites, but their relative contents there are different. The HDS sites are situated mostly on the edges rather than on the rims, because the probability of active site promotion is twice higher on the MoS_2 edges than on the rims. By contrast, there are fewer HYD sites on the edges of the active-phase crystallites than on the rims.

An increase in k_{HYD} with a growing number of MoS_2 layers per packet (Fig. 7) is attributed to the rise in the number of slow HYD sites located on the edges of the active-phase crystallites. At the same time, the increase in the number of rapid sites is sharper, because k_{DS} is more strongly dependent on $\overline{N}$ than k_{HYD}. The "delay" in the rise of k_{HYD}, as compared to k_{DS}, with growing $\overline{N}$ is responsible for the lower selectivity HYD/DS of the catalysts with a larger number of MoS_2 crystallite layers (Fig. 8). The reduction in selectivity of the catalysts promoted by Co or Ni is caused by the formation of "rapid" sites representing an aggregate of two single molybdenum sulfide clusters of which one is promoted by Ni or Co.

CONCLUSIONS

The influence that the composition of the XMo/Al_2O_3 and $Co(Ni)–XMo/Al_2O_3$ sulfide catalysts for hydrotreating prepared using the Anderson heteropoly compounds $[X(OH)_6Mo_6O_{18}]^{n-}$ (X = Co, Ni, Mn, Zn) and $[Co_2Mo_{10}O_{38}H_4]^{6-}$ has on the morphology of their active phase was studied. The average length of the active-phase particles is 3.5–3.9 nm, and the average number of MoS_2 layers per packet is from 1.4 to 2.1. The greatest number of MoS_2 layers is observed in the $Co_3–Co_2Mo_{10}HPC/Al_2O_3$ catalysts; the smallest number of these layers, in $ZnMo_6HPC/Al_2O_3$.

The catalytic properties of the synthesized samples depend both on the type and composition of the HPC and on the nature of the promoter (Ni or Co). The Co-promoted catalysts exhibit greater desulfurization activity than the Ni-promoted ones both in DBT hydrogenation and in the hydrotreating of the diesel fraction. The catalytic activity of the $Ni–XMo/Al_2O_3$ samples is, by contrast, above that of $Co–XMo/Al_2O_3$.

The morphology of the nanostructured active phase affects their catalytic properties of the catalysts. With a growing number of MoS_2 layers per active-phase packet in the Co- or Ni-promoted catalysts XMo/Al_2O_3 and $Ni(Co)–XMo/Al_2O_3$, the DBT hydrodesulfurization rate constant increases linearly for both the direct desulfurization and preliminary hydrogenation routes. At the same time, the selectivity $S_{HYD/DS}$ falls linearly with an increasing average number of MoS_2 layers. A greater reduction is observed for the catalysts $Ni–XMo/Al_2O_3$ than for $Co–XMo/Al_2O_3$.

The dependences of the catalytic properties on the active-phase morphology are consistent the dynamic model of the performance of active sites of transition metal sulfides.

ACKNOWLEDGMENTS

The work was carried out within the framework of the Federal Target Program "Research and Development in the Priority Areas of Scientific and Engineering in Russia for 2007–2013" (project no. 16.513.11.3027). A.V. Mozhaev thanks Haldor Topsøe Company for a dissertation grant. The authors are grateful to the staff of the shared facilities "Investigation of Physicochemical Properties of Compounds and Materials" of Samara State Technical University for assistance in the study of the physicochemical properties of the catalysts.

REFERENCES

1. Stanislaus, A., Marafi, A., and Rana, M.S., *Catal. Today*, 2010, vol. 153, p. 1.
2. Topsøe, H., Clausen, B.S., and Massoth, F.E., *Hydrotreating Catalysis Science and Technology*, Catalysis Science and Technology, vol. 11, Anderson, J.R. and Boudart, M., Eds., Berlin: Springer, 1996.
3. Kogan, V.M., *Doctoral (Chem.) Dissertation*, Moscow: Inst. of Organic Chemistry, 2005.
4. Startsev, A.N., *Sul'fidnye katalizatory gidroochistki: Sintez, struktura, svoistva* (Sulfide Catalysts for Hydrotreating), Novosibirsk: Geo, 2008.
5. Kogan, V.M. and Nikulshin, P.A., *Catal. Today*, 2010, vol. 149, p. 224.
6. Candia, R., Sorensen, O., Villadsen, J., Topsøe, N.-Y., Clausen, B.S., and Topsøe, H., *Bull. Soc. Chim. Belg.*, 1984, vol. 93, p. 763.
7. Topsoe, H., Candia, R., Topsøe, N.-Y., and Clausen, B.S., *Bull. Soc. Chim. Belg.*, 1984, vol. 93, p. 783.
8. Van Veen, J.A.R., Colijn, H.A., Hendriks, P.A.J.M., and van Welsenes, A.J., *Fuel Process. Technol.*, 1993, vol. 35, p. 137.
9. Bouwens, S.M.A.M., van Dijk, M.P., van der Kraan, A.M., Koningsberger, D.C., van Zon, F.B.M., de Beer, V.H.J., and van Veen, J.A.R., *J. Catal.*, 1994, vol. 146, p. 375.
10. Tomina, N.N., Pimerzin, A.A., and Moiseev, I.K., *Ross. Khim. Zh.*, 2008, vol. 52, no. 4, p. 41.
11. Eijsbouts, S., van den Oetelaar, L.C.A., and van Puijenbroek, R.R., *J. Catal.*, 2005, vol. 229, p. 352.
12. Ferdous, D., Dalai, A.K., Adjaye, J., and Kotlyar, L., *Appl. Catal., A*, 2005, vol. 294, p. 80.
13. Van Veen, J.A.R., Gerkema, E., van der Kraan, A.M., Hendriks, P.A.J.M., and Beens, H., *J. Catal.*, 1992, vol. 133, p. 112.
14. Louwen, S.P.A. and Prins, R., *J. Catal.*, 1992, vol. 133, p. 94.
15. Medici, L. and Prins, R., *J. Catal.*, 1996, vol. 163, p. 94.
16. Kishan, G., Coulier, L., Veen, J.A.R., and Niemantsverdriet, J.W., *J. Catal.*, 2001, vol. 200, p. 194.
17. Kishan, G., Coulier, L., Veen, J.A.R., and Niemantsverdriet, J.W., *J. Catal.*, 2000, vol. 196, p. 189.
18. Coulier, L., Beer, V.H.J., Veen, J.A.R., and Niemantsverdriet, J.W., *J. Catal.*, 2001, vol. 197, p. 26.
19. Al-Dalama, K., Aravind, B., and Stanislaus, A., *Appl. Catal., A*, 2005, vol. 296, p. 49.
20. Okamoto, Y., Ishihara, Sh., Kawano, M., Satoh, M., and Kubota, T., *J. Catal.*, 2003, vol. 217, p. 12.
21. Mazoyer, P., Geantet, C., Diehl, F., Loridant, S., and Lacroix, M., *Catal. Today*, 2008, vol. 130, p. 75.

22. Rana, M.S., Ramirez, J., Gutiérrez-Alejandre, A., Ancheyta, J., Cedeno, L., and Maity, S.K., *J. Catal.*, 2007, vol. 246, p. 100.

23. Lelias, M.A., van Gestel, J., Mauge, F., and van Veen, J.A.R., *Catal. Today*, 2008, vol. 130, p. 109.

24. Hensen, E.J.M., Kooyman, P.J., van der Meer, Y., van der Kraan, A.M., de Beer, V.H.J., van Veen, J.A.R., and van Santen, R.A., *J. Catal.*, 2001, vol. 199, p. 224.

25. Hensen, E.J.M., van der Kraan, A.M., de Beer, V.H.J., van Veen, J.A.R., and van Santen, R.A., *Catal. Lett.*, 2002, vol. 84, p. 59.

26. Usman, U., Takaki, M., Kubota, T., and Okamoto, Y., *Appl. Catal., A*, 2005, vol. 286, p. 148.

27. Usman, U., Kubota, T., Araki, Y., Ishida, K., and Okamoto, Y., *J. Catal.*, 2004, vol. 227, p. 523.

28. Usman, T., Kubota, I., and Hiromitsu, Y., *J. Catal.*, 2007, vol. 247, p. 78.

29. Dumeignil, F., Sato, K., Imamura, M., Matsubayashi, N., Payen, E., and Shimada, H., *Appl. Catal., A*, 2006, vol. 315, p. 18.

30. Maity, S.K., Flores, G.A., Ancheyta, J., and Rana, M.S., *Catal. Today*, 2008, vol. 130, p. 374.

31. Ding, L., Zhang, Z., Zheng, Y., Ring, Z., and Chen, J., *Appl. Catal., A*, 2006, vol. 301, p. 241.

32. Kim, H., Lee, J.J., and Moon, S.H., *Appl. Catal., B*, 2003, vol. 44, p. 287.

33. Klimov, O.V., Pashigreva, A.V., Fedotov, M.A., Kochubey, D.I., Chesalov, Y.A., Bukhtiyarova, G.A., and Noskov, A.S., *J. Mol. Catal. A: Chem.*, 2010, vol. 322, p. 80.

34. Klimov, O.V., Pashigreva, A.V., Bukhtiyarova, G.A., Budukva, S.V., Fedotov, M.A., Kochubey, D.I., Chesalov, Yu.A., Zaikovskii, V.I., and Noskov, A.S., *Catal. Today*, 2010, vol. 150, p. 196.

35. Klimov, O.V., Fedotov, M.A., Pashigreva, A.V., Budukva, S.V., Kirichenko, E.N., Bukhtiyarova, G.A., and Noskov, A.S., *Kinet. Catal.*, 2009, vol. 50, no. 6, p. 867.

36. Breysse, M., Geantet, C., Afanasiev, P., Blanchard, J., and Vrinat, M., *Catal. Today*, 2008, vol. 130, p. 3.

37. Kraleva, E., Spojakina, A., Jiratova, K., and Petrov, L., *Catal. Lett.*, 2006, vol. 112, p. 203.

38. Spojakina, A., Kraleva, E., Jiratova, K., and Petrov, L., *Appl. Catal., A*, 2005, vol. 288, p. 10.

39. Spojakina, A., Jiratova, K., Kostova, N., Kocianova, J., and Stamenova, M., *Kinet. Catal.*, 2003, vol. 44, no. 6, p. 813.

40. Palcheva, R., Spojakina, A., Tyuliev, G., Jiratova, K., and Petrov, L., *Kinet. Catal.*, 2007, vol. 48, p. 847.

41. Shafi, R., Siddiqui, M.R.H., Hutchings, G.J., Derouane, E.G., and Kozhevnikov, I.V., *Appl. Catal., A*, 2000, vol. 204, p. 251.

42. Pawelec, B., Mariscal, R., Fierro, J.L.G., Greenwood, A., and Vasudevan, P.T., *Appl. Catal., A*, 2001, vol. 206, p. 295.

43. Blanchard, P., Lamonier, C., Griboval, A., and Payen, E., *Appl. Catal., A*, 2007, vol. 322, p. 33.

44. Lizama, L. and Klimova, T., *Appl. Catal., B*, 2008, vol. 82, p. 139.

45. Cabello, C.I., Munoz, M., Payen, E., and Thomas, H.J., *Catal. Lett.*, 2004, vol. 92, p. 69.

46. Cabello, C.I., Cabrerizo, F.M., Alvarez, A., and Thomas, H.J., *J. Mol. Catal. A: Chem.*, 2002, vol. 186, p. 89.

47. Botto, I.L., Cabello, C.I., and Thomas, H.J., *Mater. Chem. Phys.*, 1997, vol. 47, p. 37.

48. Cabello, C.I., Botto, I.L., and Thomas, J.H., *Appl. Catal., A*, 2000, vol. 197, p. 79.

49. Pettiti, I., Botto, I.L., Cabello, C.I., Colonna, S., Faticanti, M., Minelli, G., Porta, P., and Thomas, H.J., *Appl. Catal., A*, 2001, vol. 220, p. 113.

50. Mazurelle, J., Lamonier, C., Lancelot, C., Payen, E., Pichon, Ch., and Guillaume, D., *4th Int. Symp. on Molecular Aspects of Catalysis by Sulfides*, Doorn, Netherlands, 2007, p. 17 .

51. Mazurelle, J., Lamonier, C., Payen, E., and Guillaume, D., *Catal. Today*, 2008, vol. 130, p. 41.

52. Lamonier, C., Martin, C., Mazurelle, J., Harle, V., Guillaume, D., and Payen, E., *Appl. Catal., B*, 2007, vol. 70, p. 548.

53. Nikulshin, P.A., Tomina, N.N., Pimerzin, A.A., Stakheev, A.Yu., Mashkovsky, I.S., and Kogan, V.M., *Appl. Catal., A*, 2011, vol. 393, pp. 146–152.

54. Nikulshin, P.A., Tomina, N.N., Pimerzin, A.A., Kucherov, A.V., and Kogan, V.M., *Catal. Today*, 2010, vol. 149, p. 82.

55. Tomina, N.N., Nikul'shin, P.A., and Pimerzin, A.A., *Pet. Chem.*, 2008, vol. 48, no. 2, p. 92.

56. Spojakina, A.A., Kraleva, E.Y., and Jiratova, K., *Kinet. Catal.*, 2010, vol. 51, no. 3, p. 385.

57. Nikitina, E.A., *Geteropolisoedineniya* (Heteropoly Compounds), Moscow: Goskhimizdat, 1962.

58. Stepin, B.D., Gorshtein, I.G., Blyum, G.E., Kurdyumov, G.M., and Ogloblina, I.P., *Metody polucheniya osobo chistykh neorganicheskikh veshchestv* (Methods of Obtaining Special-Purity Inorganic Compounds), Leningrad: Khimiya, 1969.

59. *Handbuch der preparativen anorganischen Chemie*, von Brauer, G., Ed., Stuttgart: Ferdinand Enke, 1981.

60. Klyuchnikov, N.G., *Rukovodstvo po neorganicheskomu sintezu* (Guide to Inorganic Synthesis), Moscow: Khimiya, 1965.

61. Nikul'shin, P.A., *Cand. Sci. (Chem.) Dissertation*, Moscow: Inst. of Organic Chemistry, 2009.

62. Van Veen, J.A.R., Hendriks, P.A.J.M., Andrea, R.R., Romers, E.J.G.M., and Wilson, A.E., *J. Phys. Chem.*, 1990, vol. 94, p. 52.

63. Daage, M., Chianelli, R.R., and Ruppert, A.F., *Stud. Surf. Sci. Catal.*, 1993, vol. 75, p. 571.

64. Chianelli, R.R., Daage, M., and Ledoux, M.J., *Adv. Catal.*, 1994, vol. 40, p. 177.

65. Daage, M. and Chianelli, R.R., *J. Catal.*, 1994, vol. 149, p. 414.

66. Berhault, G., Rosa, M.P., Mehta, A., Yacaman, M.J., and Chianelli, R.R., *Appl. Catal., A*, 2008, vol. 345, p. 80.